Multi-mode Waveguides with Tailored Dispersion - a Way for Coherent and Dispersion-Free Propagation of Classical and Quantum Optical Signals

C. A. Valagiannopoulos,[1] A. Mandilara,[1] S. A. Moiseev,[2,3] and V. M. Akulin[3,4]

[1] *Department of Physics, School of Science and Technology, Nazarbayev University, 53, Kabanbay batyr Av., Astana, 010000, Republic of Kazakhstan.*

[2] *Quantum Center, Kazan National Research Technical University, 10 K. Marx, Kazan, 420111, Russia.*

[3] *Laboratoire Aimé-Cotton CNRS UMR 9188, L'Université Paris-Sud et L'École Normale Supérieure de Cachan, Bât. 505, Campus d'Orsay, 91405 Orsay Cedex, France*

[4] *Institute for Information Transmission Problems of the Russian Academy of Science, Bolshoy Karetny per. 19, Moscow, 127994, Russia.*

We show how by a tailored breaking of the translational symmetry in waveguides and optical fibers one can control chromatic dispersions of the individual modes at any order and thereby overcome the problem of coherent classical and quantum signal transmission at long distances. The method is based on previously developed quantum control techniques and provides analytic solution for a general class of models. In practice, this requires mode couplers and the possibility of tailoring the dispersion laws around the operating frequency. We develop the method for spatial modes of a waveguide and we further apply the technique to design dispersion-less propagation for the polarization modes of a uniaxial material.

PACS numbers: 03.67.Hk Quantum communication, 42.50.-p Quantum optics, 42.79.Sz Optical communication systems, multiplexers, and demultiplexers , 42.81.-i Fiber optics

Transmission of information at long distances via multi-mode optical fibers/waveguides is limited by the necessity to compensate for the spread in package arrival times caused by the discrepancy in the group velocities of different waveguide modes. At the same time the dispersion effects need to be compensated for each of the modes. Is there a way to overcome these problems and construct a multi-mode waveguide with identical group velocities of different modes and no quadratic dispersion? Here we show that by breaking the translation invariance in a specific way one can accomplish such a task.

There is a vast amount of work [1]-[2] related the dispersion problem and the method developed here has unavoidable overlap with several of them. The method that we suggest provides dispersion along the fiber/waveguide by perturbing the translation symmetry similarly to fiber Bragg gratings [3] and the tailoring of photonic band structures techniques [4]. This also assumes availability of mode couplers which have been extensively used in the design of dispersion compensation filters for two [7] and higher number of modes [8]. Furthermore, for the development of the method we borrow previously developed ideas for implementing quantum control [5] over compact semigroups [6]. The main contribution of our method is that the discrepancy in the mode dispersion laws can be compensated *up to any predetermined order* k of the Taylor expansion around a given operational signal frequency, in complete analogy with the regime of Quantum Error Protection [5],[9] and similar to the regime of Dynamic Decoupling [10]. Moreover in the case where advanced tailoring of the dispersions' laws is possible, the method can be extended to compensate for higher than quadratic order dispersions.

The structure of this paper is the following. In Section I we illustrate and develop the method at a simple example of two spatial mode waveguide of a rectangular profile. The exact analytical expressions for the mode dispersions permit to suggest an explicit spatial distribution of ideal scatterers coupling the modes and which act as perturbations backing the translational invariance. More specifically, we derive $4k$ non-linear algebraic equations in analytic form that determine the positions $\{L_1, \ldots, L_M\}$ of $M = 4k$ scatterers, such that signals on the two modes propagate in phase, synchronously and without dispersion up to k-th order of Taylor expansion. At the same time, we emphasize that, by analogy, the same problem can be solved for any finite number N of modes by finding numerically a proper distribution of $M = N^2 k$ generic [11] ideal scatterers along the perturbation period. In Section II we apply the method for designing dispersion-less propagation in an actual structure with imperfect scattering carried out by flakes of graphene in a uniaxial background. With this example, we explicitly show how the method can be efficiently adjusted to given realistic conditions and materials.

I. PROPOSED METHOD WITH IDEALIZED SCATTERERS

Consider a rectangular $a \times b$ waveguide with conducting walls, shown in Fig. 1 a). If we consider a frequency-dependent refraction index $n(\omega)$, then the mode wavevectors $A_{l,j}$, and z-components of the vector potential of the electromagnetic field mode functions, as these defined up to normalization constants $\alpha_{l,j}$,

$$A_{l,j}(x,y,z) = \alpha_{l,j} \sin\left(\pi l \frac{x}{a}\right) \sin\left(\pi j \frac{y}{b}\right) e^{i(\kappa_{l,j} z - \omega t)} \quad (1)$$

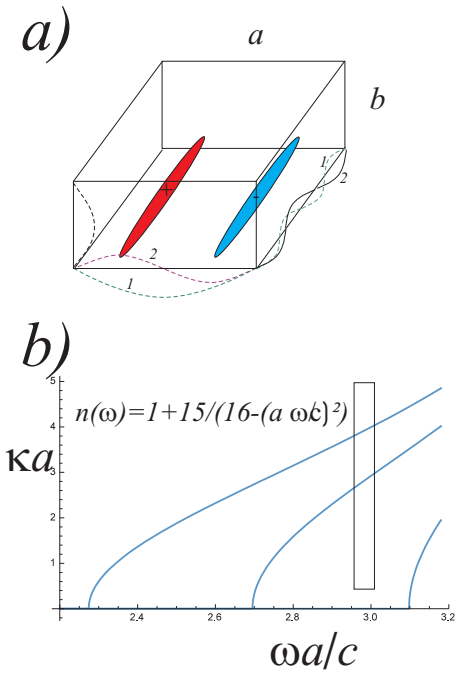

FIG. 1: *a)* Rectangular $a\times b$ waveguide with conducting walls. Co-factors of the mode functions given by Eq.(1) for two first modes are shown by dashed lines. By ellipses we show a scatterer, which is a pair of smooth positive (+) and negative (-) perturbations of the refraction index that have a length longer that the modes wavelength still remaining shorter than the inverse of the mode wavevectors difference. *b)* Dispersion law for the two first modes for the case $a = 2b$ and in the presence of the frequency dependent refraction index $n(\omega)$ has a domain near $\omega = 3c/a$ (shown by a rectangle) where the second derivatives $\partial^2\kappa/\partial\omega^2$ of the first and the second waveguide modes have compensate each for the other. As a result, Eq.(5) for $n(\omega) = 1 + 15/(16 - (a\omega/c)^2)$ yields Taylor expansion $F_I(\omega) = 3.36984 + 5.23733(a\omega/c - 2.98307) + O((a\omega/c - 2.98307)^3)$

follow different dispersion laws

$$\kappa_{l,j}(\omega) = \sqrt{n^2(\omega)\left(\frac{\omega}{c}\right)^2 - \left(\frac{l\pi}{a}\right)^2 - \left(\frac{j\pi}{b}\right)^2}. \quad (2)$$

For $a = 2b$, around the frequency $\omega_0 \cong 3c/a$, there exist only two waveguide modes $(j = 1, l = 1)$ and $(j = 1, l = 2)$, as it is shown in Fig. 1b). Moreover, by a proper choice of the dependence $n(\omega)$ shown in Fig. 1b), one can find a regime where the dispersion $\partial^2\kappa/\partial\omega^2$ at ω_0 for the first mode is opposite to that of the second one. Propagation of a two-mode signal at $\omega \cong \omega_0$ along a waveguide of length L results in accumulation of the mode phases factors, that can be written in matrix form as multiplication of the two-component mode amplitude vector by a matrix

$$\widehat{U}_L = e^{-iL\left(F_z(\omega)\widehat{\sigma}_z + F_I(\omega)\widehat{I}\right)}. \quad (3)$$

The logarithm of $\widehat{U}_L$ is proportional to the sum of the Pauli matrix $\widehat{\sigma}_z$ with a frequency dependent pre-factor

$$F_z(\omega) = \frac{\kappa_{1,1}(\omega) - \kappa_{2,1}(\omega)}{2} \quad (4)$$

and the identity matrix $\widehat{I}$ also multiplied by a frequency dependent pre-factor

$$F_I(\omega) = \frac{\kappa_{1,1}(\omega) + \kappa_{2,1}(\omega)}{2}. \quad (5)$$

For $\omega \cong \omega_0$ the coefficient $F_I(\omega)$ does not contain the quadratic dispersion term $(\omega - \omega_0)^2$ in its Taylor expansion as presented in Fig. 1 caption.

Now we assume that at some point L_z along the propagation line locates a scatterer which flips the amplitudes of the modes. This can be achieved, for instance, by antisymmetric Gaussian perturbation of the refraction index shown in Fig. 1a). By choosing the size δn of the refraction index perturbation

$$\delta n(x,y,z) = \delta n(e^{-\frac{(x-x_0)^2}{\alpha^2} - \frac{(y-y_0)^2}{\alpha^2} - \frac{(z-L_z)^2}{\beta^2}} - e^{-\frac{(x-a+x_0)^2}{\alpha^2} - \frac{(y-y_0)^2}{\alpha^2} - \frac{(z-L_z)^2}{\beta^2}}),$$

the perturbation matrix elements

$$V_{l,l} = \int \delta n(x,y,z) A_{l,1}(x,y,z) A_{l,1}(x,y,z) dxdydz = 0$$
$$V_{1,2} = \int \delta n(x,y,z) A_{1,1}(x,y,z) A_{2,1}(x,y,z) dxdydz \neq 0 \quad (6)$$

can be set in such a way that the mode scattering matrix

$$\widehat{S} = \exp(i\widehat{s}) \quad (7)$$

with the scattering action matrix [12]

$$\widehat{s} = F_x(\omega)\widehat{\sigma}_x \quad (8)$$

is proportional to the Pauli matrix $\widehat{\sigma}_x$ with a coefficient

$$F_x(\omega) = \frac{\pi}{2} + F'_x(\omega_0)(\omega - \omega_0) + \frac{F''_x(\omega_0)}{2}(\omega - \omega_0)^2 + \ldots \quad (9)$$

For a smooth enough perturbation $(\beta\kappa \gg 1)$, the back scattering is negligible. The assumption $F_x(\omega_0) = \frac{\pi}{2}$ is not crucial and as we show in Section II one can even use this angle as an additional free parameter in the problem. We also note here that frequency dependence mode-couplers, as fiber gratings [13], can fit to this general model of scatterers.

We now come to the key idea of our method. The combined mode transformation matrix that describes scattering and then propagation for distance L, reads

$$\widehat{U}_L\widehat{S} = e^{-iLF_I(\omega)\widehat{I}} e^{-iL\widehat{\sigma}_z F_z(\omega)} e^{i\widehat{\sigma}_x F_x(\omega)}. \quad (10)$$

We repeat such a transformation 3 times with 3 different length parameters L_1, L_2, L_3, and require that up to the common phase factor $e^{-i(L_1+L_2+L_3)F_I(\omega)}$ the resulting transformation matrix

$$\begin{aligned}\widehat{T} = e^{-iL_3\widehat{\sigma}_z F_z(\omega)} e^{i\widehat{\sigma}_x F_x(\omega)} e^{-iL_2\widehat{\sigma}_z F_z(\omega)} \\ e^{i\widehat{\sigma}_x F_x(\omega)} e^{-iL_1\widehat{\sigma}_z F_z(\omega)} e^{i\widehat{\sigma}_x F_x(\omega)}\end{aligned} \tag{11}$$

equals to a nondegenerate square root of the identity matrix [6] with the accuracy of the order of $(\omega-\omega_0)^3$. Formally this requirement implies that $\mathrm{Det}\widehat{T} = -1$ while the linear coefficient $c_1(L_1, L_2, L_3, \omega)$ in the characteristic polynomial

$$\mathrm{Det}\left[\widehat{T} - \lambda\widehat{I}\right] = \lambda^2 + c_1(L_1, L_2, L_3, \omega)\lambda - 1 \tag{12}$$

vanishes together with its two first frequency derivatives, that is

$$\begin{aligned} c_1(L_1, L_2, L_3, \omega_0) &= 0, \\ \frac{\partial}{\partial\omega} c_1(L_1, L_2, L_3, \omega)\Big|_{\omega=\omega_0} &= 0, \\ \frac{\partial^2}{\partial\omega^2} c_1(L_1, L_2, L_3, \omega)\Big|_{\omega=\omega_0} &= 0. \end{aligned} \tag{13}$$

In such a situation the $\widehat{T}^2$ becomes the identity matrix up to a cubic correction

$$\widehat{T}^2 = e^{\widehat{\sigma}O\left[(\omega-\omega_0)^3\right]}, \tag{14}$$

where $\widehat{\sigma}$ is a 2×2 matrix of norm one. Therefore both waveguide modes have identical phase shifts $2(L_1+L_2+L_3)F_I(\omega)$, which does not contain quadratic terms in their Taylor expansion over frequency thus resulting in the signal propagation with identical group velocity in both modes and with no quadratic dispersion. Furthermore, in practice the $\mathrm{Det}\widehat{T} = -1$ requirement does not need to be imposed since $\left|\mathrm{Det}\widehat{T}\right| = 1$ always holds for unitary matrices. In this case, an additional frequency-independent global phase will appear on $\widehat{T}^2$ that we will ignore in the rest of the discussion for two modes −this phase can be easily recompensed.

Now we let us turn to our particular example where we have an explicit analytic expression for the coefficient $c_1(L_1, L_2, L_3, \omega_0)$

$$\begin{aligned} c_1 = 2\left[\cos F_x(\omega) - \cos^3 F_x(\omega)\right] \\ \{\cos\left[F_z(\omega)(L_1 - L_2 - L_3)\right] + \\ \cos\left[F_z(\omega)(L_1 + L_2 - L_3)\right] + \\ \cos\left[F_z(\omega)(L_1 - L_2 + L_3)\right]\} \\ - 2\cos^3 F_x(\omega)\cos\left[F_z(\omega)(L_1 + L_2 + L_3)\right] \end{aligned} \tag{15}$$

while according to Eq.(4) $\cos F_x(\omega) \propto (\omega-\omega_0)$, and therefore, to be consistent within the order of approximation, the term containing $\cos^3 F_x(\omega)$ has to be ignored. This makes the first of Eqs.(13) fulfilled as the identity, and thus the system becomes degenerate consisting of just two equations

$$\begin{aligned} 0 &= \cos\left[X_1 - X_2 - X_3\right] + \cos\left[X_1 + X_2 - X_3\right] \\ &\quad + \cos\left[X_1 - X_2 + X_3\right], \\ 0 &= (X_1 - X_2 - X_3)\sin\left[X_1 - X_2 - X_3\right] + \\ &\quad (X_1 + X_2 - X_3)\sin\left[X_1 + X_2 - X_3\right] + \\ &\quad (X_1 - X_2 + X_3)\sin\left[X_1 - X_2 + X_3\right], \end{aligned} \tag{16}$$

on three variables $F_z(\omega_0)L_1 \to X_1$, $F_z(\omega_0)L_2 \to X_2$, $F_z(\omega_0)L_3 \to X_3$. The system Eq.(16) has a continuous family of solutions easy to find numerically. One can get a countable number of solutions if the system is complemented by the additional physical requirement $(L_1+L_2+L_3)F_I(\omega_0) = (X_1+X_2+X_3)F_I(\omega_0)/F_z(\omega_0) = 2m\pi$. Then, for $m = 10$, and coefficients $F_I(\omega_0) = 3.36984$, $F_z(\omega_0) = 0.549151$ suggested by the Taylor expansions around the frequency $\omega_0 = 2.98307c/a$, we numerically find one of many possible solutions, $X_1 = 2.10269$, $X_2 = 0.776642$, $X_3 = 7.35977$. This solution indeed yields the transfer matrix

$$\left(\widehat{U}_{L_1}\widehat{S}\widehat{U}_{L_2}\widehat{S}\widehat{U}_{L_3}\widehat{S}\right)^2 = e^{i195.3037\frac{\omega-\omega_0}{c/a}+\widehat{O}} \tag{17}$$

over a period of length $2(L_1+L_2+L_3) = 18.645a$, where $\widehat{O} = i(185.11\widehat{I} - 4.08\widehat{\sigma}_y + 4.48\widehat{\sigma}_x)\left(\frac{\omega-\omega_0}{c/a}\right)^3$ a cubic correction. We note here that the degeneracy in the system Eq.(13) is lifted when either the requirement $F_x(\omega_0) = \frac{\pi}{2}$ or the assumption Eq.(8) is relaxed.

To better ensure the identity of propagating signals in different modes, the order k of the Taylor remainder can be increased and, in principle, done as high as needed,– the system Eq.(13) for such a case has to be extended to incorporate more variables L_i and require vanishing of all higher-order derivatives $\partial^{k-1}c_1/\partial\omega^{k-1}$ at $\omega = \omega_0$. In contrast, in order to eliminate also the cubic and higher-order dispersion in the common phase of the modes, one has to properly tailor the frequency dependence of the refraction index $n(\omega)$, a task which can be possibly addressed in the discipline of metamaterials. In the case where no explicit analytical derivatives of the mode dispersion are available all the derivatives entering Eqs.(13) have to be taken numerically.

We now briefly consider the general formulation of the problem in the case of N modes with different dispersion laws $\kappa_l(\omega)$. The aim is to achieve a tailored breaking of translational symmetry such as all modes have identical dispersion laws up to the k-th order of Tailor expansion. As earlier, we consider a sequence of mode scattering transformations

$$\widehat{T}(\{L_l\}, \omega) = \prod_{l=1}^{kN}\left(e^{-iL_l\widehat{\phi}(\omega)}e^{i\widehat{s}(\omega)}\right) \tag{18}$$

where $\widehat{s}(\omega)$ is a generic [11] frequency dependent $N \times N$ Hermitian scattering action matrix, and $\widehat{\phi}(\omega)$ is a real traceless diagonal $N \times N$ matrix with the elements $\phi_{ll}(\omega) = \kappa_l(\omega) - \frac{1}{N}\sum_{j=1}^{N}\kappa_j(\omega)$, which describes the mode phase difference accumulation per unit waveguide distance. The average mode wavevector $\kappa_0(\omega) = \frac{1}{N}\sum_{l=1}^{N}\kappa_l(\omega)$ contributes with a global phase $\kappa_0(\omega)\sum_{l=1}^{N}L_l$, which is factored out from the product Eq.(18). Let us assume that by tuning the material refraction index one gets the desired analytic properties $\kappa_0(\omega)$ at $\omega = \omega_0$. One thus have to find length intervals $\{L_l\}$ such that $\widehat{T}$ would be a nondegenerate N-th root of the identity matrix up to the terms $O\left((\omega-\omega_0)^k\right)$.

To this end we consider the characteristic polynomial

$$\mathrm{Det}\left[\widehat{T}-\lambda\widehat{I}\right] = \lambda^N + \sum_{n=1}^{N-1} c_n\left(\{L_l\},\omega\right)\lambda^n + e^{i\varphi(\{L_l\},\omega)} \tag{19}$$

and require, that at $\omega = \omega_0$ all coefficients c_n vanish together with all their derivatives till $(k-1)$-th order. In addition, we require that $\varphi\left(\{L_l\},\omega_0\right) = 2\pi q$ with $q < N$ an integer number, and also all derivatives to vanish including $(k-1)$-th order. All together we impose kN conditions on kN variables $\{L_l\}$, – a system of nonlinear algebraic equations to be solved numerically for given $\widehat{\phi}(\omega)$ and $\widehat{s}(\omega)$. Once a solution is found, the repetition of the scattering sequence N-times, corresponding to the matrix $\widehat{T}^N\left(\{L_l\},\omega\right) = e^{\widehat{O}\left[(\omega-\omega_0)^k\right]}$ results in the required propagation with a common phase $\kappa_0(\omega)\sum_{l=1}^{N}L_l$, which can be in principle controlled by a proper tailoring of the refraction index $n(\omega)$.

II. MATERIALIZATION WITH ACTUAL MEDIA

A. Presentation of the Configuration

In the aforementioned analysis, we have presented the method by considering, as a model example, the spatial modes of a waveguide. In this context, it is difficult to think of structures conforming the strict conditions of perfect scattering (7)-(8), even though the possibility of tailoring the dispersion relations of the waveguide is realistic. In this Section, we provide a second example of applicability of the method, addressing different issues that may arise in practice and considering realistic structures in the mode conversion of the input signal.

To simplify the approach, we consider propagation into unbounded media (instead of a waveguide); thus, the role of two modes is played by the two polarizations of the incoming field which are vertical to each other. The background medium treats differently each direction of electric field which means that is uniaxial [14], namely is characterized by a diagonal permittivity matrix. Furthermore, since we are referring to real-world systems, the scattering angles (which now express linear polarization tilts) are considered small to avoid significant backscattering. It has been found [15], that a magnetically-biased graphene flake exhibits that property of polarization rotation and therefore it is utilized in our consideration. For the operational frequencies that this effect is recorded, the tilt is not changing substantially and thus is assumed to be frequency-independent. Under these assumptions and as we show below, the first equation of Eqs.(13) dictates that the sum of all the scattering angles of the half-scheme (see Fig. 2) should be equal to $\pi/2$.

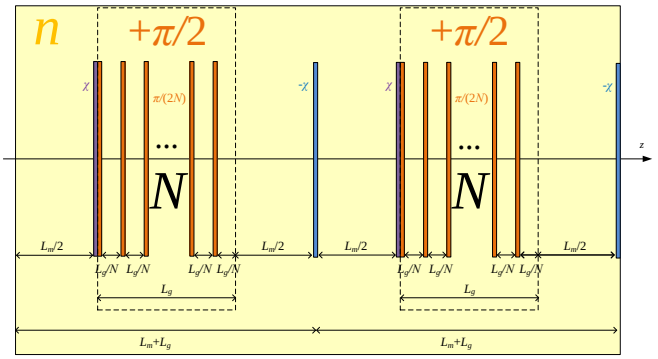

FIG. 2: The physical configuration of the proposed structure. The overall system is comprised of two identical components each of which contains $(N+2)$ graphene flakes suitably distributed along a length $(L_m + L_g)$ of the z axis into the background medium of refractive index n.

After extensive parametric checks, we have concluded that the minimal configuration which can make a total transfer matrix $\hat{T}^2 \cong \hat{I} \Leftrightarrow \hat{T} \cong \sqrt{\hat{I}}$, is that depicted in Fig. 2. As the light arrives from the left side, it propagates into our background medium for a total length $L_m/2$ before meeting a graphene sheet of scattering angle χ. To this end, it is inserted to a stack of N identical graphene flakes with distance L_g/N between two neighboring ones; the graphenes are suitably polarized and doped to achieve an overall Faraday rotation of $\pi/2$. The outcoming signal propagates for another length $L_m/2$ before being subjected to an opposite tilt of $(-\chi)$. As indicated above, to avoid transmissivity issues, the polarization tilt χ is taken low and for simplicity equal to that of each graphene sheet of the stack: $\chi = \pi/(2N)$. The same half-structure repeats itself to form a planar stack of multiple layers which provides dispersion-free propagation.

B. Uniaxial Medium with Lorentz Dispersions

An electric field $\vec{\mathcal{E}}(z,t)$ with a vector lying on the xy plane which propagates along the z axis into a uniaxial medium, characterized by refractive indexes (n_x, n_y) along the corresponding axes, is written as an inverse Fourier transform: $\vec{\mathcal{E}}(z,t) = \int_{-\infty}^{+\infty}\vec{E}(z,\omega)A(\omega)e^{+i\omega t}d\omega$.

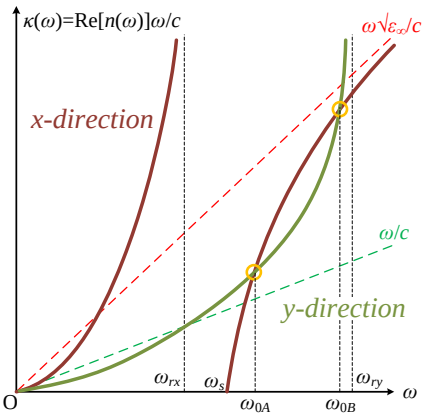

FIG. 3: Schematic graphs of the (real parts of) propagation constants along the two axes (x, y) of the uniaxial medium as function of frequency ω.

The complex phasor of the electric field is given by [16]:

$$\vec{E}(z,\omega) = \hat{x}S_x e^{-i\frac{\omega}{c}n_x(\omega)z} + \hat{y}S_y e^{-i\frac{\omega}{c}n_y(\omega)z}, \qquad (20)$$

while $A(\omega)$ is the Fourier transform of the time-dependent profile of the input signal which is assumed to be concentrated around a central operating frequency ω_0. The amplitudes (S_x, S_y) determine the sort (linear or elliptical) and the tilt angle of the polarization [17].

It is clear that each electric component "sees" a different permittivity and gets affected independently by each of the refractive indexes $n_x(\omega), n_y(\omega)$ due to the uniaxial nature of the background medium. For this reason, each transverse component of the electric field defines a mode with different dispersion relation $n_{x,y}(\omega)$. We assume that the frequency-dependent refractive indexes follow simple Lorentz models [18] and are written as follows:

$$n_x(\omega) = \sqrt{\varepsilon_\infty + \frac{\omega_p^2}{\omega_{rx}^2 - \omega^2}}, \qquad (21)$$

$$n_y(\omega) = \sqrt{1 + \frac{\omega_p^2}{\omega_{ry}^2 - \omega^2}}. \qquad (22)$$

Assume that the two permittivities are characterized by the same plasma frequency ω_p for brevity, while the high-frequency limits of the dielectric constants are different (ε_∞ for the x direction and 1 for the y direction). The resonance frequencies $\omega_{rx,y}$ are also different and, since $\varepsilon_\infty > 1$, we need to assume $\omega_{ry} > \omega_{rx}$ for reasons that will become obvious later in the analysis. Note that for a lossless medium (which is our case because we study the propagation into it), the quantities $n_{x,y}$ of (21) and (22) are either positive or purely imaginary; we are obviously interested for frequencies where both are positive: $n_{x,y} > 0$.

Since the polarization direction (angle) of our electric field expresses the weights of each of the two superimposed modes, it should be retained as linear during the free propagation into our background medium; this is possible only into an isotropic environment. However, our material is uniaxial; thus, we demand $n_x = n_y$ only at $\omega = \omega_0$. In Fig. 3, we schematically show the variation of the quantities $\kappa_{x,y}(\omega) = \mathrm{Re}[n_{x,y}(\omega)\ \omega/c]$ with respect to the frequency ω. Each curve begins from the origin ($\omega = 0$) and takes all the positive values to become infinite at $\omega = \omega_{rx,y}$. For $\omega \gtrsim \omega_{rx,y}$ the represented quantity becomes imaginary since the value under the root in (21),(22) turns to very negative from very positive. However, if ω passes a larger threshold ($\omega_s > \omega_{rx}$ for the x direction), the refractive index gets again positive and remains so (no matter how high the frequency is – for $\omega \to \infty$ behaves like its linear asymptote). As also indicated in Fig. 3, when one has $\varepsilon_\infty > 1$ (as we assumed), the two refractive indexes can be equal only when $\omega_{ry} > \omega_{rx}$ and such an equality is achieved for operational frequencies within the interval $\omega_s < \omega < \omega_{ry}$. At the frequency $\omega_s^2 = \omega_{rx}^2 + \omega_p^2/\varepsilon_\infty$, the refractive index of x axis gets nullified; for $\omega > \omega_s$ its curve $n_x(\omega)$ has two common points with the graph of $n_y(\omega)$ at the frequencies ω_{0A} and ω_{0B} whose explicit expressions are not shown here for brevity.

Therefore, we have two alternative central frequencies $\omega = \omega_{0A,B}$ at which the isotropy demand is well-served. Nevertheless, an additional constraint is related to the sign of the second derivative of propagation constants $\kappa''_{x,y}$. The whole dispersion-neutralization concept described in the Section I is based on the assumption that the quantities $\kappa''_x(\omega)$ and $\kappa''_y(\omega)$ are opposite in the vicinity of $\omega = \omega_0$. Accordingly, we would like the functions $\kappa_x(\omega)$ and $\kappa_y(\omega)$ to have opposite second derivatives at their common points $\omega = \omega_{0A,B}$. A necessary but not sufficient condition for it, is to have the same first derivatives; in particular, for $\kappa''_x(\omega_0) = -\kappa''_y(\omega_0)$, the two curves should be mirror-symmetric with respect to their common tangent. In other words, the equation $\kappa_x(\omega) = \kappa_y(\omega)$ should have a double root at $\omega = \omega_{0A} = \omega_{0B}$. Such a condition becomes feasible for $\omega_p^2 = (\varepsilon_\infty - 1)(\omega_{ry}^2 - \omega_{rx}^2)/4$ and leads to operational frequency $\omega_0^2 = (\omega_{ry}^2 + \omega_{rx}^2)/2$. Thus, one can search for the desired regime $\kappa''_x(\omega_0) = -\kappa''_y(\omega_0)$ in the parametric vicinity of these values.

The transmission matrix of a two-port network (each port corresponds to one polarization mode), which is comprised only by a length L of a medium, as this described above, is obviously written as:

$$\hat{U}_L = \begin{bmatrix} e^{-i\kappa_x(\omega)L} & 0 \\ 0 & e^{-i\kappa_y(\omega)L} \end{bmatrix}. \qquad (23)$$

C. Graphene Flakes as Imperfect Scatterers

As it is well-known [15], an one-atom-thick graphene flake, being doped with electric charge carriers (electrons) at graphene conduction band with energy μ_c (chemical potential), exhibits specific surface conductivity γ

[19]. If, additionally, it gets biased normally to its surface by a DC magnetic field B_0, the graphene sheet becomes anisotropic (and non-reciprocal) because its conductivity matrix $\hat{\gamma}$ acquires non-zero off-diagonal elements ($\gamma_{xy} = -\gamma_{yx} = \gamma_O(\omega)$) apart from the diagonal ones ($\gamma_{xx} = \gamma_{yy} = \gamma_D(\omega)$). The corresponding formulas, obey the Kubo model [19] and are not reproduced here for brevity.

Let us consider a single graphene flake into the aforementioned uniaxial background medium with refractive indexes $n_{x,y}(\omega)$, which is excited by the electric field of (20). If one imposes the necessary boundary conditions [15] for continuous tangential electric fields $\vec{n} \times (\vec{E}_2 - \vec{E}_1) = \vec{0}$ and discontinuous tangential magnetic fields $\vec{n} \times (\vec{H}_2 - \vec{H}_1) = \hat{\gamma} \cdot \vec{E}_2$, one obtains the following transfer matrix

$$\hat{S} = \frac{2}{(2n_x + \eta_0\gamma_D)(2n_y + \eta_0\gamma_D) + \eta_0^2\gamma_O^2} \begin{pmatrix} n_x(2n_y + \eta_0\gamma_D) & -n_y\eta_0\gamma_O \\ n_x\eta_0\gamma_O & n_y(2n_x + \eta_0\gamma_D) \end{pmatrix}, \quad (24)$$

where η_0 is the wave impedance of free space and $\vec{n}$ the unitary vector normal to the surface pointing from side 1 to side 2. This matrix connects the two polarization components of the electric field from both sides of the graphene boundary. Note that for an opposite magnetic bias ($B_0 \to -B_0$), the conductivity matrix of the flake gets transposed ($\hat{\gamma} \to \hat{\gamma}^T$ because γ_O changes sign); therefore, the same happens to the transfer matrix (24) of the graphene sheet ($\hat{S} \to \hat{S}^T$) [20].

D. Calculation of the Overall Transmissivity

By taking into account the transfer matrices (23), (24), one can write down the total transfer matrix $\hat{P}$ of the overall configuration shown in Fig. 2 as follows:

$$\hat{P} = \left(\hat{S}^T \hat{U}_{\frac{L_m}{2}} \left(\hat{U}_{\frac{L_g}{N}} \hat{S} \right)^N \hat{S} \hat{U}_{\frac{L_m}{2}} \right)^2. \quad (25)$$

The symbol $\hat{S}$ is used for the scattering matrix of a single graphene flake that rotates the polarization direction at $\omega = \omega_0$, by angle $\chi = \pi/(2N)$. If one excludes from (25) the common phase for both polarization components $e^{-i(\kappa_x(\omega)+\kappa_y(\omega))(L_m+L_g)\hat{I}}$, which for $\omega \cong \omega_0$ does not contain the quadratic dispersion term, one obtains the analogous to Eq.(11) relation:

$$\hat{T} \cong e^{i\frac{\pi}{2N}\hat{\sigma}_y} e^{-ih(\omega)\frac{L_m}{2}\hat{\sigma}_z} e^{-ih(\omega)L_g\hat{\sigma}_z - i\frac{\pi}{2}\hat{\sigma}_y} e^{-i\frac{\pi}{2N}\hat{\sigma}_y} e^{-ih(\omega)\frac{L_m}{2}\hat{\sigma}_z}, \quad (26)$$

where for $\omega \cong \omega_0$, the Taylor expansion is used: $h(\omega) = (\kappa_x'(\omega_0) - \kappa_y'(\omega_0))(\omega - \omega_0)/2 + \kappa_x''(\omega_0)(\omega - \omega_0)^2$.

The derivation of (26) relies on the assumptions: (i) the tilt angle $\chi = \pi/(2N)$ is small so that we have almost perfect transmissivity from the graphene flake, (ii) the number N of graphene flakes is large enough so that the Trotter's formula is applicable $\left(e^{-ih(\omega)\frac{L_g}{N}\hat{\sigma}_z - i\frac{\pi}{2N}\hat{\sigma}_y}\right)^N \cong e^{-ih(\omega)L_g\hat{\sigma}_z - i\frac{\pi}{2}\hat{\sigma}_y}$, (iii) the signal is concentrated around $\omega = \omega_0$, (iv) the tilt in the polarization angle $\chi = \pi/(2N)$ of the linearly polarized field inflicted by the graphene is practically independent from frequency ω across the operational bandwidth around ω_0 [21].

We repeat the method described in Section I, namely, we demand that the characteristic polynomial Det $\left[\widehat{T} - \lambda\widehat{I}\right]$ does not possess, in the vicinity of $\omega = \omega_0$, a first-order term with respect to λ. Accordingly, we obtain from the third condition in (13), namely the demand for: $\frac{\partial^2}{\partial\omega^2} c_1(L_1, L_2, L_3, \omega)\Big|_{\omega=\omega_0} = 0$, the following

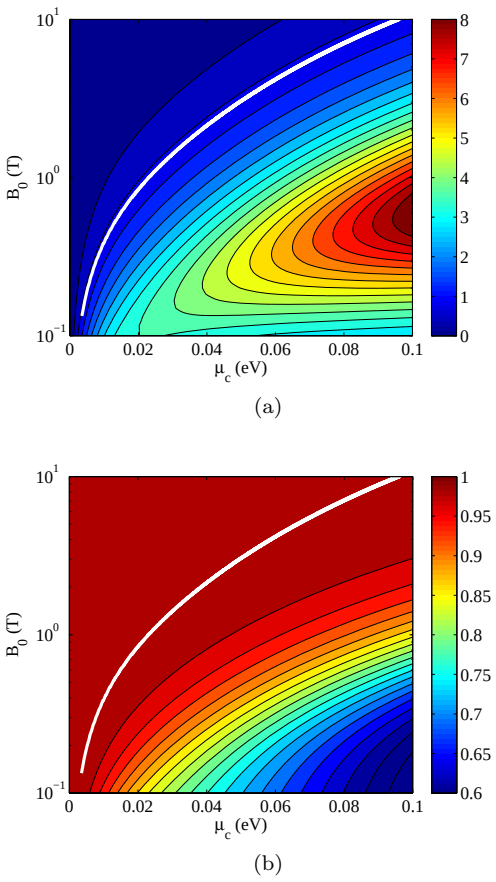

FIG. 4: The: (a) tilt angle of the linear polarization in degrees and (b) normalized squared amplitude, that characterizes the transmitted wave as functions on the chemical potential μ_c required for the doping of graphene and the magnetic bias B_0. The white line shows the combinations of (μ_c, B_0) which lead to polarization tilt $\chi = \pi/(2N)$ for $N = 100$. The conductivity of graphene has been computed with use of Kubo model [19] with $v_F \cong 10^6$ m/sec Fermi group velocity of the electrons in the hexagonal lattice, $T \cong 300$ K room temperature and $\tau \cong 0.2$ psec transport scattering time of the electrons.

relation connecting the lengths L_m, L_g:

$$\frac{L_m}{L_g} = \frac{2\csc(2\chi)}{\pi} \cdot \left(2\cos^2\chi + \sqrt{\cos\chi\,(3\cos\chi + \cos(3\chi) + 2\pi\sin\chi)}\right), \quad (27)$$

where $\chi = \pi/(2N)$. One can easily verify that the first two conditions in (13) are identically satisfied when the total scattering angle for the half-scheme is $\pi/2$ as it is for our case. This degeneracy stems from the conditions of: (i) uniaxial medium that dictates that $\kappa_x(\omega_0) = \kappa_y(\omega_0)$ and (ii) frequency independence tilt angles χ of the graphene flakes. In this way, for a fixed (large) number N of graphene flakes equally distributed within a length L_g, we obtain via Eq.(27) the necessary size of the background medium L_m so that the scheme illustrated in Fig. 2 leads to dispersion-less and coherent propagation.

E. Numerical Simulations

The polarization tilt through a graphene flake has been recorded mainly at the microwaves [15] and thus our operational frequency belongs within the interval 10 GHz $< \omega/(2\pi) <$ 60 GHz. The chemical potential is kept small (below 0.1 eV) since we are interested for small tilts $\chi = \pi/(2N)$, while the magnetic bias is permitted to take large (> 1 T) or even huge and unrealistic (> 10 T) values since it helps us demonstrating our concept. When it comes to the background medium, we have noticed that better final outcome is obtained when the resonant frequencies are not very close each other. Therefore, we can make a pre-selection of $\omega_{rx} = 10(2\pi)$ Grad/sec and $\omega_{ry} = 60(2\pi)$ Grad/sec. As far as the high-frequency permittivity along the x axis is concerned, it can take an ordinary value above unity: $\varepsilon_\infty = 2.5$ [22]. Finally, as mentioned above, the number of graphene layers is selected quite high: $N = 100$. By carefully evaluating the double derivatives of $\kappa''_{x,y}(\omega)$, we conclude that the condition $\kappa''_x(\omega_0) = -\kappa''_y(\omega_0)$ is achieved for a common plasma frequency of Lorentz models $\omega_p \cong 36.19(2\pi)$ Grad/sec with central operational frequency $\omega_0 \cong 42.07(2\pi)$ Grad/sec.

In Figs 4, we examine the behavior of a graphene flake into the aforementioned uniaxial medium, at the oscillating frequency ω_0. In Fig. 4(a), we show the tilt angle (in degrees) that a linearly polarized incident field experiences by passing through a graphene sheet of chemical potential μ_c and magnetic bias B_0. It is clear that the polarization rotation is a growing function of μ_c and gets maximized for a specific B_0. The white line corresponds to combinations of (μ_c, B_0) which give a tilt equal to $\chi = \pi/(2N) = \pi/200 \cong 0.9^o$ and thus are suitable for our specific application. One observes that for every single bias (except for some very low B_0), there is always a doping degree μ_c which constitutes a working point. In Fig. 4(b), we show the same white line but on the map of the transmissivity of a single graphene flake.

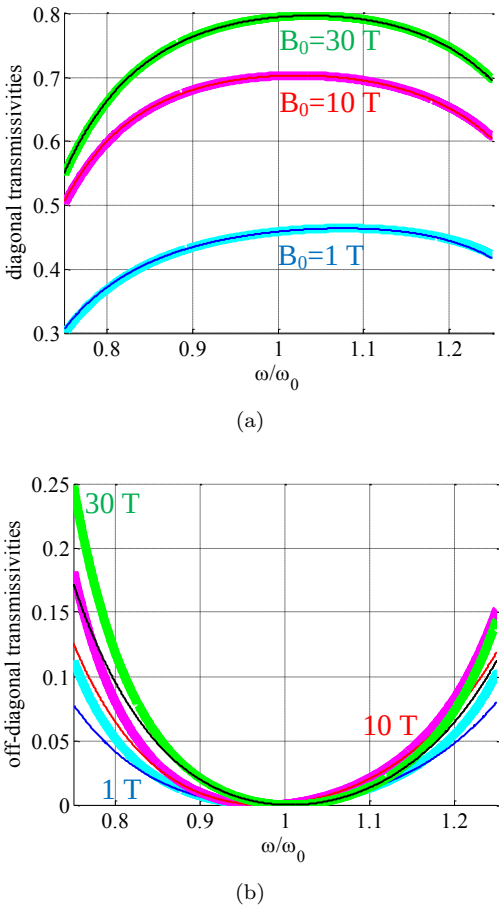

FIG. 5: The: (a) diagonal (ideally 1 in the vicinity of $\omega = \omega_0$) and (b) off-diagonal (ideally 0 in the vicinity of $\omega = \omega_0$) transmissivities of the overall structure in Fig. 2 as function of the normalized frequency ω/ω_0. Several magnetic bias are considered combined with suitable chemical potential dictated by the white line of Figs 4 ($\mu_c \cong 0.0229$ eV for $B_0 = 1$ T, $\mu_c \cong 0.0953$ eV for $B_0 = 10$ T and $\mu_c \cong 0.1671$ eV for $B_0 = 30$ T). The rest of graphene parameters are identical to those of Figs 4.

It is clearly recorded that the transmission coefficient is very high; this finding is a positive indicator that the described concept for minimal dispersion may work well in the described real-world configuration.

However, this high transmissivity indicated by Fig. 4(b) does not automatically give an overall power output close to 100%. This is referred to a single graphene flake alone into our background medium; however, the device of Fig. 2, we have clusters of (N) of these sheets. Therefore, we should check the transmission through the entire structure. If we assume the thickness of the graphene stack equal to $L_g = 500$ nm (lattice period $L_g/N = 5$ nm, for a tilt $\chi = \pi/200$ (corresponding to $N = 100$), we obtain from (27) that the length L_m is found equal to: $L_m \cong 40.8$ μm.

In Figs 5, we pick three combinations of graphene doping and bias (μ_c, B_0) which lead to polarization tilt by

$\chi = \pi/(2N)$ (two of them are within the limits of the maps of Figs 4) and represent the squared magnitudes of the four elements of matrix $\hat{P}$ from (25). We use light-colored thick lines and dark-colored thin lines in order to represent each couple (diagonal or off-diagonal) of quantities. Ideally, the diagonal of them should be equal to 1 around $\omega = \omega_0$ and the off-diagonal ones should vanish in the vicinity of $\omega = \omega_0$. Note that we expect neither the diagonal elements to be equal each other (because the network is not symmetric) nor the off-diagonal ones to be equal each other (because the network is not reciprocal).

In Fig. 5(a), the diagonal transmissivities are shown with respect to the operational frequency ω normalized by the central frequency ω_0 for various bias $B_0 = 1, 10, 30$ T. In all the three cases we observe a substantial stability of the response in the neighborhood of $\omega = \omega_0$, which means that our dispersion-free structure can support wide-band signals. As anticipated, the transmission through the structure gets deteriorated far from $\omega = \omega_0$ because the device has been designed to operate at this oscillation frequency. Notice that the two diagonal elements of $\hat{P}$ have almost identical magnitude variation with respect to ω; this feature can be attributed to the effective "averaging" performed by the multiple layers which mitigates the overall asymmetry. It is also remarkable that despite the very high transmission revealed by Fig. 4(b), the total transmissivity is much weaker due to the presence of numerous graphene sheets (as implied above). Most importantly, we see that larger magnetic fields B_0 accomplish better results which means that the transmission along the white line of Fig. 4(b) is not equally high; even very small changes to the behavior of a single scatterer has a significant outcome to the total structure (comprised of $(2N + 2)$ scatterers).

In Fig. 5(b), we show the corresponding (squared magnitudes of the) off-diagonal elements of the matrix $\hat{P}$ defined in (25) as functions of ω/ω_0. It is clear that all the quantities vanish at $\omega = \omega_0$ and acquire substantial values far from the central frequency for the obvious reason mentioned above. Following the trend of the diagonal elements, the quantities in Fig. 5(b) are, on average, larger as B_0 increases; however, in all the three of the considered cases, the magnitudes of off-diagonal terms are much smaller than the respective diagonal ones (Fig. 5(a)). It should be also stressed that, unlike the diagonal ones in Fig. 5(a), the two off-diagonal elements differ each other; this is the definition of of non-reciprocity [15] and is attributed to the presence of external magnetic bias.

Therefore, we can conclude that in a realistic scheme like that in Fig. 2, one can emulate dispersion-free propagation for a suitably modulated signal around frequency $\omega = \omega_0$. Two electromagnetic entities are required: (i) A properly designed uniaxial medium whose refractive indexes $n_x(\omega), n_y(\omega)$ follow common Lorentz dispersion models. (ii) Graphene flakes with specific doping (with chemical potential μ_c) and magnetic bias (B_0).

III. DISCUSSION

Chromatic dispersion is one of the main problems [23] in optical communications over long distances and many works have been devoted to this subject [1]-[2]. In classical single-mode optical networks the most common method seems to be at this point the dispersion compensating fibers. In the multi-mode scenario the techniques are somehow different, and there is a number of elegant suggestions, e.g. [24], [25], including ones [8] which are based on the conversion of the signal between different modes, as the current work does, and on the tailoring of the dispersion laws.

Concerning dispersion compensation in single-mode quantum signals, the direct extension of classical methods to quantum signals -containing low number of photons, is under question [26] since these may induce additional source of photon losses. Quantum solitons [27] provide a solution to this problem but on the other hand these require elaborate means of preparation.

The method that we describe in this work provides analytic expressions which can be employed to eliminate quadratic dispersion at any Taylor order and even compensate dispersion at higher orders. The results are applicable to both classical and quantum multi-mode networks however it seems to be more of interest in the latter case. The first interesting point of the method is that under the condition of weak scattering, the method does not induce photon losses on the signal. The second advantage is that the proposed method can produce phase matching conditions along extended distances and thereby induce nonlinear coupling between the quantum fields of different modes even for a typically weak nonlinear permeability. This result that seems negative at first look, may pave new methods in multi-mode quantum communication, where entanglement can be generated 'on the way' and used for error-protection of signals against photon losses. This idea is to be further developed in a future work.

Acknowledgement

AM acknowledges financial support from the Ministry of Education and Science of the Republic of Kazakhstan (Contract # 339/76 − 2015). AM is also thankful to CCQCN at University of Crete for their hospitality and partial financial support by the European Union Seventh Framework Programme (EU/FP7-REGPOT-2012-2013-1) under Grant No. n316165. VA thanks G. A. Kabatiansky for attracting his attention to this problem.

[1] *Fiber Based Dispersion Compensation*, edited by S. Ramachandran, (Springer-Verlag, New York, 2007).

[2] Agrawal G. P., *Fiber-Optic Communication Systems*, 3rd ed., (Wiley, 2002).

[3] F. Ouellette, Opt. Lett. 12, 847 (1987).

[4] K. Hosomi and T. Katsuyama, IEEE J. Quantum Electron. 38, 7 (2002); A. Yu. Petrov and M. Eich, Appl. Phys. Lett. 85, 4866 (2004).

[5] V. M. Akulin, Dynamics of Complex Quantum Systems, (Springer, New York, 2014).

[6] G. Harel and V. M. Akulin, Phys. Rev. Lett. 82, 1 (1999).

[7] C. D. Poole, J. M. Wiesenfeld, A. R. McCormick, and K.T. Nelson, Opt. Lett. 17, 985 (1992); M. Eguchi, M. Koshiba, and Y. Tsuji, J. Lightw. Technol. 14, 2387 (1996); M. Eguchi, J. Opt. Soc. Am. B 18, 737 (2001).

[8] C. D. Poole, J. M. Wiesenfeld, D. J. DiGiovanni, and A. M. Vengsarkar, J. Lightw. Technol. 12, 1745 (1994).

[9] Michael A. Nielsen and Isaac L. Chuang, *Quantum Computation and Quantum Information*, (Cambridge University Press, 2000).

[10] L. Viola, E. Knill and S. Lloyd, Phys. Rev. Lett. 82, 2417 (1999).

[11] The term "generic enough" has an exact meaning: the scattering action matrix $\widehat{s}$ (example Eq.(8) for $su(2)$) and the waveguide mode phase accumulation matrix $\widehat{\phi}$ (example - co-factor of L_1 in the exponent of the right hand side of Eq.(3)) have to satisfy the so-called bracket generation condition - their all-order commutators should span all the relevant algebra of generators of the group of the mode amplitude transformations.

[12] We do not dwell here on the relation between the scattering matrix and the perturbation, which is given by the well-known Lipman-Schwinger equation.

[13] R. Kashyap, *Fiber Bragg Gratings*, (Academic Press, San Diego, CA, 1999); C. D. Poole, C. D. Townsend, and K. T. Nelson, J. Lightw. Technol. 9, 598 (1991).

[14] A. Sihvola, *Electromagnetic Mixing Formulas and Applications*, (Institution of Electrical Engineers, London 1999).

[15] D. L. Sounas and C. Caloz, IEEE Trans. Microwave Theory Tech. 60, 901 (2012).

[16] C. A. Balanis, *Advanced Engineering Electromagnetics*, (Wiley, 2012).

[17] S. J. Orfanidis, *Electromagnetic Waves and Antennas*, freely available online at: ece.rutgers.edu/˜orfanidi/ewa.

[18] R. W. Ziolkowski, IEEE Trans. Antennas. Propag. 51, 1516 (2003).

[19] G. W. Hanson, J. Appl. Phys. 103, 064302 (2008).

[20] C. A. Valagiannopoulos, Microw. Opt. Technol. Lett 55, 16 (2013).

[21] M. Mattheakis, C. A. Valagiannopoulos and E. Kaxiras Phys. Rev. B 94, 201404 (2016).

[22] C. A. Valagiannopoulos, N. L. Tsitsas and A. H. Shilova, Trans. Geosci. Rem. Sens. 54, 3697 (2016).

[23] E. Agrell *et al*, J. Opt. 18, 063002 (2016).

[24] S. Fan and J. M. Kahn, Opt. Lett. 30, 135 (2005).

[25] X. Shen, J. M. Kahn, and M. A. Horowitz, Opt. Lett. 30, 2985 (2005).

[26] S. Fasel, N. Gisina, G. Ribordy, and H. Zbinden, Eur. Phys. J. D 30, 143 (2004); M. Suda, T. Herbst, and A. Poppe, Eur. Phys. J. D 42, 139 (2007).

[27] P. D. Drummond, R. M. Shelby, S. R. Friberg and Y. Yamamoto, Nat. 365, 307 (1993); G. P. Agrawal, *Nonlinear Fiber Optics* (Academic Press, San Diego 2001); G. Leuchs, Ch. Silberhorn, F. König, P. K. Lam, A. Sizmann and N. Korolkova, in *Quantum Information with Continuous Variables,* edited by S.L. Braunstein and A.K. Pati, (Kluwer Academic Publishers, Dodrecht 2002).